Thermal stability of ultrathin ZrO_2 films and structure determination of $ZrSi_2$ islands on Si(100)

Frank Schönbohm,* Christian Rolf Flüchter, Daniel Weier, Tobias Lühr, Ulf Berges, Sven Döring, and Carsten Westphal
Experimentelle Physik 1, Technische Universität Dortmund, Otto-Hahn-Str. 4, D-44221 Dortmund, Germany and DELTA, Technische Universität Dortmund, Maria-Goeppert-Mayer-Str. 2, D-44221 Dortmund, Germany
(Received 24 July 2009; revised manuscript received 23 September 2009; published 20 October 2009)

The temperature dependence of ultrathin ZrO_2 films on clean (2×1)-reconstructed Si(100) was studied by means of x-ray photoelectron spectroscopy and photoelectron diffraction (XPD). ZrO_2 films with a thickness of approximately 11 Å were grown by electron-beam evaporation. At temperatures of 650 °C and above it was found that the zirconia (ZrO_2) films were transformed into $ZrSi_2$. The temperature region of structural transformation could be narrowed to the range from 650 to 725 °C. During the formation of $ZrSi_2$ all oxygen was removed from the sample surface. After annealing at 725 °C neither zirconia nor silicon oxide could be verified on the sample. Scanning electron microscopy (SEM) measurements showed the $ZrSi_2$ being arranged in islands on the surface after annealing. From the combined spectroscopy, SEM, and XPD analysis a model for the internal structure of $ZrSi_2$ is proposed.

DOI: 10.1103/PhysRevB.80.165323 PACS number(s): 81.05.Je, 79.60.Dp, 61.05.js, 61.05.jh

I. INTRODUCTION

Following Moore's law electronic devices undergo a continuous downscaling where their size is reduced from one processor generation to the next. This miniaturization becomes problematic if the SiO_2 gate dielectric thickness is reduced below ~2 nm. It is well known that semiconductor devices with insulating SiO_2 layers below ~2 nm loose their efficiency due to an increased tunneling current.[1] One way to keep the so-called leakage current low is the growth of a sufficient thick gate dielectric on the semiconductor in order to suppress tunneling. On the other hand a thin gate dielectric is desired for a high gate capacitance of the metal oxide semiconductor field-effect transistor (MOSFET). An increased capacitance as well as a significant reduction in the tunnel leakage current can be achieved by substituting the presently used SiO_2 by materials with higher dielectric constants. During the last years many research activities were performed in order to investigate possible alternatives. Because of their high dielectric constant the compounds are often referred to as *high-k* materials.[2] Some promising candidates which probably could substitute SiO_2 are HfO_2 and ZrO_2.[3] Presently, the thermal stability of ultrathin zirconia films on Si surfaces is not clear. During the production process of SiO_2 based MOSFET semiconductor devices temperatures of approximately 1050 °C are required for dopant activation,[1] while the ZrO_2 film already collapses at much lower temperatures.

Because of its importance to future applications we studied ultrathin zirconia films on a Si(100) surface. *In situ* x-ray photoelectron spectroscopy (XPS) measurements were performed and the system's evolution during annealing at increased temperatures was analyzed. The temperature range of the structure transition from ZrO_2 to $ZrSi_2$ was determined by a stepwise annealing process. As a result we report the transition occurring between 650 to 725 °C.

Scanning electron microscopy (SEM) measurements showed that due to the annealing process $ZrSi_2$ islands are generated on the sample's surface.[4] In order to determine the internal structure of the $ZrSi_2$ islands x-ray photoelectron diffraction (XPD) patterns were recorded and compared to model simulations. We present a first structure model for the $ZrSi_2$ islands obtained from the combined analysis of the photoelectron diffraction patterns, SEM, and spectroscopy data. The knowledge of the internal structure of these islands is necessary in order to understand their electronic properties and the driving forces of island growth.

II. EXPERIMENT

Sample preparation, XPS, and XPD measurements were performed *in situ* in an UHV chamber at beamline 11 of the synchrotron radiation facility DELTA (TU Dortmund, Germany). During all experiments and preparation processes the base pressure was below 5×10^{-11} mbar. The chamber is equipped with an electron analyzer, a low-energy electron diffraction (LEED) system, an electron-beam evaporator (EBE), and a manipulator which allows sample annealing and movement under UHV conditions. The Si(100) samples were annealed by direct current. For the *in situ* film preparation the samples were flashed at approximately 1050 °C in order remove the covering native oxide layer. A slow temperature decrease over a time period of about 10 min resulted in a (2×1) reconstructed Si(100) surface. The surface reconstruction was checked by LEED and the absence of surface impurities was verified by means of XPS. Thin ZrO_2 films were evaporated by EBE on the surface directly after sample cleaning.

The ZrO_2 evaporation material is contaminated by residual Hf since Hf and Zr are difficult to separate due to their similar chemical properties.[5] The amount of HfO_2 in the applied ZrO_2 is about 2–4 % according to the manufacturer's datasheet.[6] In addition, a very small amount of yttrium could be verified on the sample after evaporation which was not mentioned by the manufacturer,[6] since Y is often used to stabilize the ZrO_2.[5]

All XPS spectra and the XPD patterns were recorded at a photon energy of $h\nu=320$ eV. This energy was chosen in order to obtain a high surface sensitivity and to separate Zr 3*d* signals from the Si(LVV)-Auger intensities.[7] A Shirley

background[8] was removed from all photoelectron spectra and their intensity was normalized to the synchrotron's photon flux.

The XPD patterns display the electron intensity modulation in the half space above the sample due to the electron diffraction at near neighbor atoms around the emitter. The electron diffraction patterns provide information about the emitters local environment.[9–12]

A direct surface structure determination from the recorded XPD patterns is not possible because the electron's phase information is lost during the measurement. Thus a model structure was used for comparison to simulated diffraction patterns.[13,14] The calculations were performed using the MSPHD package which was developed for simulations of diffraction patterns at low kinetic electron energies.[15] For the comparison of the experimental and the simulated patterns a reliability-factor[16] (R-Factor) was introduced as a numeric measure. The R-Factor is defined as

$$R = \sum_{\theta,\phi} \frac{[\chi_{exp}(\theta,\phi) - \chi_{calc}(\theta,\phi)]^2}{[\chi^2_{exp}(\theta,\phi) + \chi^2_{calc}(\theta,\phi)]} \quad (1)$$

resulting in an interval $0 \leq R \leq 2$, where $\chi(\theta,\phi)$ is the intensity modulation caused due to the diffraction of the electrons.

SEM pictures from the sample surface were recorded after annealing at temperatures of 800 °C. The measurements were conducted *ex situ* at the Institute for Analytical Sciences[17] (ISAS). The samples were studied by recording secondary electrons with an Everhart-Thornley detector.[18] The primary energy of the scanning electrons was set to 15 keV.

III. RESULTS

ZrO_2 was evaporated onto the silicon wafer within a total time of ~75 min. The evaporation process was interrupted every 15 min in order to record XPS spectra of the Si 2*p* and Zr 3*d* intensities. The photoelectron spectra are presented in Figs. 1(a) and 1(b). In Fig. 1(a) a shift of ΔE_{kin} approximately −0.2 eV of the Si 2*p* signal is observed during evaporation. The shift depends on the film thickness and is caused due to the loss of band gap states associated with the (2×1)-reconstructed surface.[19] In addition, a decrease in the Si 2*p* intensity as a function of the accumulated evaporation time is displayed in Fig. 1(a). The intensity decrease is caused by the inelastic damping of electrons in the covering ZrO_2 film. The growth of the ZrO_2 film itself is displayed in Fig. 1(b) represented by the growing Zr 3*d* intensity. In the Zr 3*d* signal an energy shift as a function of film thickness is observed, too. For the first deposition with a deposition time of 15 min the signal is to weak for a reliable determination of the kinetic energy of the Zr 3*d* signal. Thus the Zr 3*d* signal position observed after 30 min deposition time was used for reference for observing the energy shift as a function of film thickness. We found an energy shift of $\Delta E_{kin} = -0.43$ eV for the Zr 3*d* signal in the spectrum recorded after 75 min. For even thicker Zr films energy shifts up to 0.6 eV were reported in literature previously.[20]

The Zr-film thickness was calculated from the inelastic damping of the Si 2*p* signal with respect to the gain of the Zr 3*d* intensity.[21] After 75 min of accumulated evaporation time the deposited ZrO_2 reached a thickness of approximately 11 Å. Thus we estimate a growth rate of ~2–3 Å per evaporation cycle of 15 min. This rather low evaporation rate is a direct consequence of the low ZrO_2 vapor pressure even at elevated temperatures. After 30 min of ZrO_2 evaporation time the LEED pattern of the Si(2×1) reconstruction disappears. The amorphous zirconia overlayer is indicated by the absence of any diffraction spots. At this point the thickness of the zirconia film has reached ~5 Å.

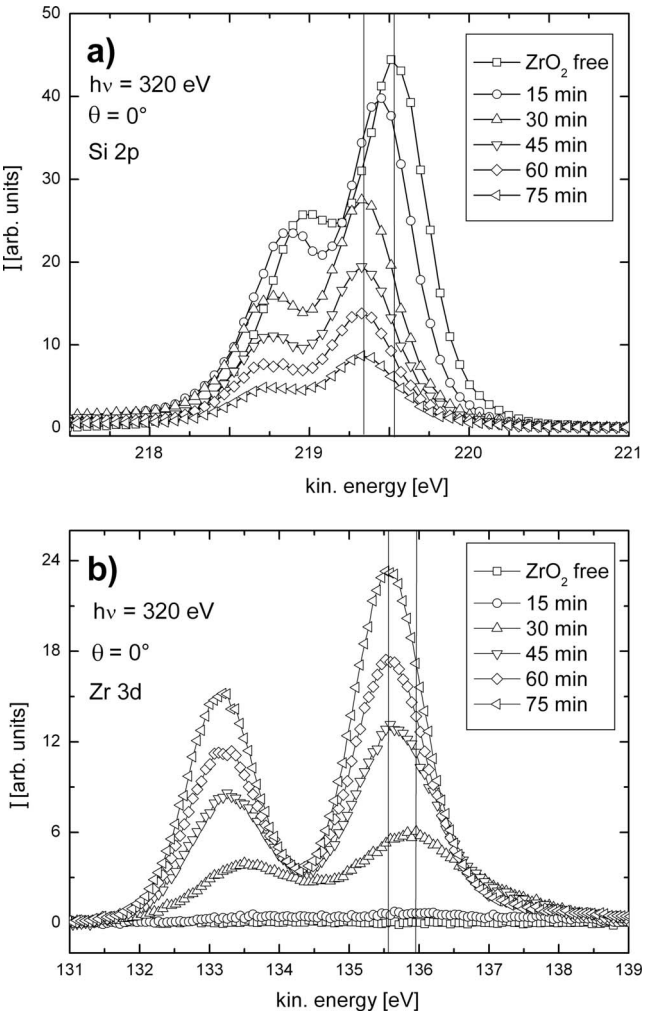

FIG. 1. Photoemission spectra recorded during subsequent ZrO_2 deposition. The indicated time refers to the total evaporation time. (a) The Si 2*p* signal decreases while (b) the Zr 3*d* intensity increases as a function of the total evaporation time.

Figure 2 displays the Zr 3*d* intensity after the total evaporation time of 75 min, together with a curve resolution of the recorded signal into its components. The spectrum shows the signal being broadened to its high kinetic-energy side, clearly indicating the formation of suboxides during evaporation. Besides $ZrO_2(Zr^{4+})$ the suboxides $Zr_2O_3(Zr^{3+})$, ZrO (Zr^{2+}), and $Zr_2O(Zr^{1+})$ can be verified in the spectrum. In the curve resolution the known binding energy separation of the Zr 3*d* doublet[22] of 2.39 eV and the intensity ratio[23] of $\frac{2}{3}$ was set constant. Furthermore, the chemical shifts of the Zr_2O_3 and the Zr_2O signal with respect to the ZrO_2 binding energy

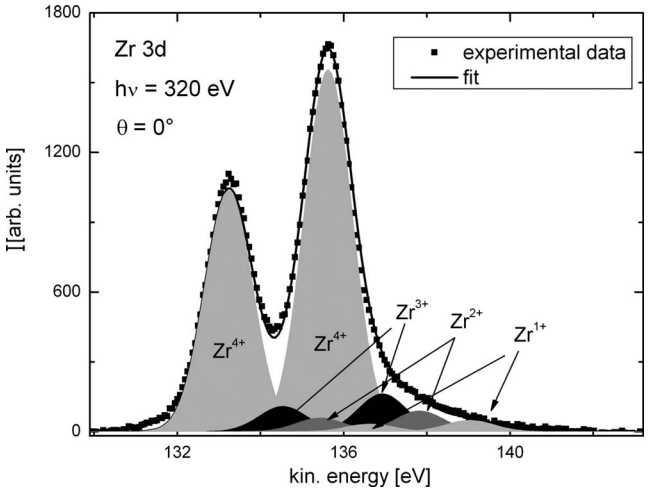

FIG. 2. Curve resolution of the ZrO_2 photoelectron signal into components. The spectrum was recorded from a sample with 75 min of accumulated evaporation time. The signal broadening at the higher kinetic-energy side is caused by the formation of Zr suboxides on the sample surface.

were set to 1.3 and 3.4 eV, respectively.[24] Free parameters for the curve resolution were the shift of Zr^{2+} with respect to the position of ZrO_2 and the intensities of the four different zirconium oxides. Additionally the formation of Si oxides was observed, too.

ZrO_2 films were studied as a function of temperature in a temperature range from 500 to 750 °C. Therefore samples were annealed for 10 min at the respective temperature, followed by a cooling period of ≈45 min. Subsequently Si 2*p* and the Zr 3*d* spectra were recorded. Figure 3(a) shows the evolution of the Si 2*p* intensity for an annealing series from 500 to 750 °C. For temperatures below 600 °C the spectrum remains unchanged. At a temperature of 650 °C a new component arises in the spectra indicated by a broadening in the Si 2*p* signal. Its intensity shift with respect to the bulk signal is approximately ΔE_{kin}=+0.5 eV which could be referred to the formation of $ZrSi_2$ on the sample.

As a further experimental observation the Si 2*p* signal remains nearly constant below 650 °C, whereas an increase in the signal is displayed for higher annealing temperatures. The steady increase in the Si 2*p* intensity was observed with every heating cycle above 650 °C up to the highest applied temperature of 750 °C. In the last spectrum recorded after annealing at 750 °C the integrated Si 2*p* signal has almost reached the same intensity as observed for the clean Si(100) sample displayed in Fig. 1(a). Also, a LEED pattern denoting the Si(2×1) surface reconstruction is reappearing at the same time. The newly formed $ZrSi_2$ component remains on the sample after annealing at 750 °C, but it is superposed by the dominant Si 2*p* bulk intensity.

The Zr 3*d* spectra presented in Fig. 3(b) show a strong binding energy shift of ΔE_{kin}=+3.7 eV as a function of annealing temperature. For annealing temperatures below 650 °C the Zr 3*d* spectrum remains unchanged. For elevated temperatures above 650 °C the Zr 3*d* intensity assigned to ZrO_2 decreases and a new component arises at higher kinetic energies. At temperatures of 725 and 750 °C the photoelectron signal of ZrO_2 vanishes completely while the chemically shifted $ZrSi_2$ component remains in the spectra.

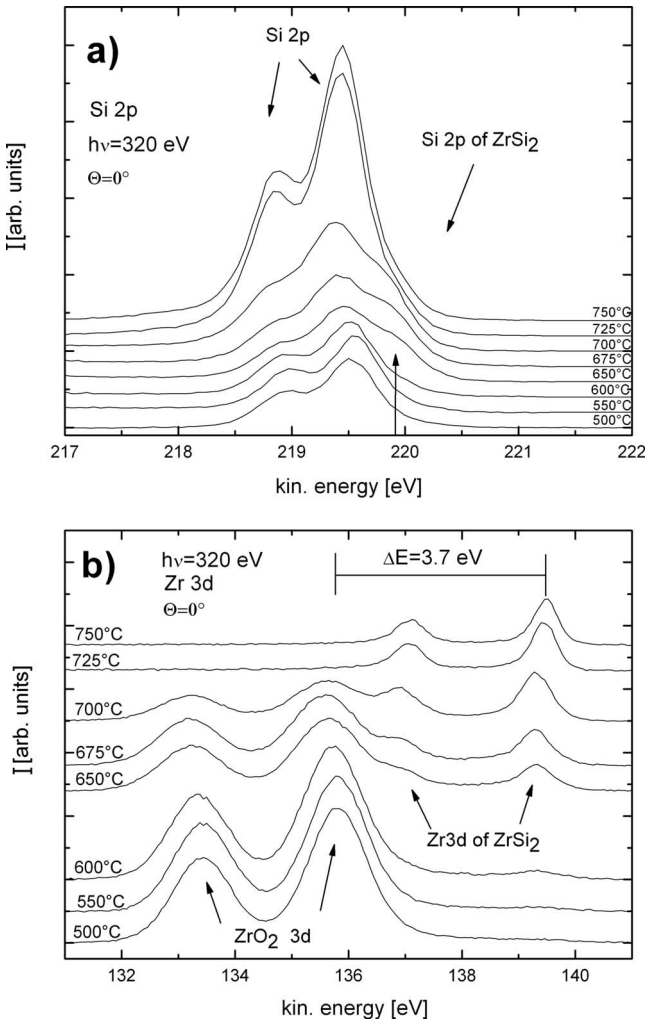

FIG. 3. (a) Si 2*p* and (b) Zr 3*d* intensities after annealing at different temperatures. In the Si 2*p* spectra a shoulder arises at the high kinetic-energy side due to the formation of $ZrSi_2$. For heating cycles above 650 °C the intensity associated with the ZrO_2 3*d* level decreases. At temperatures above 725 °C no oxygen is left on the sample and the ZrO_2 3*d* intensity vanishes completely. Simultaneously the $ZrSi_2$ component is formed on the sample surface chemically shifted by ΔE=3.7 eV to higher kinetic energies (b).

Figure 4 displays overview spectra of the sample surface after annealing at 600 and 750 °C, recorded with an energy of $h\nu$=1486.6 eV. After annealing at 650 °C oxygen is completely desorbed from the surface while the Zr signal is reduced by a small amount only. Furthermore, a closer inspection shows that the Zr 3*s*, Zr 3*p*, and Zr 3*d* intensities were shifted to higher kinetic energies due to the formation of $ZrSi_2$ at the surface. A possible formation of $ZrSiO_4$ as a result of the annealing process can be excluded since no oxygen could be detected in the spectrum in Fig. 4.

The clear increase in the Si XPS signal compared to the Zr signal accompanied by the formation of a sharp (2×1) LEED pattern can be explained by the assumption that at least parts of the Si substrate are free of any adsorbate layers and that these regions of the Si surface contribute to the

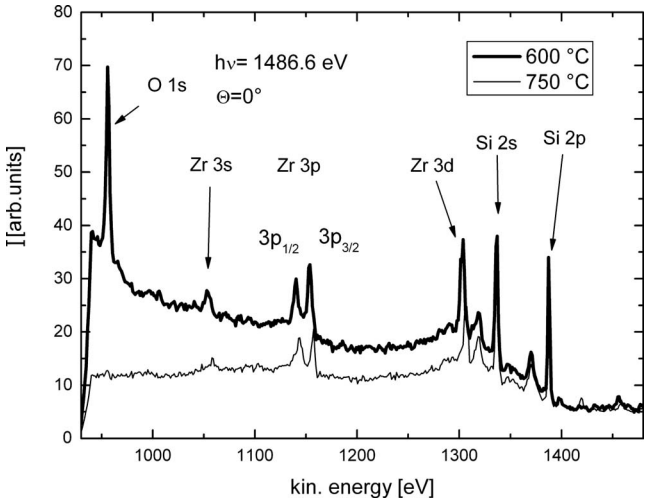

FIG. 4. Overview spectra after annealing at 600 and 750 °C. The spectra were recorded with a photon energy of $h\nu = 1486.6$ eV. For temperatures above 725 °C the O 1*s* component vanishes completely.

(2×1) LEED diffraction pattern. A possible mechanism for this observation could either be a zirconium diffusion into the substrate or an island formation of zirconium at the surface revealing the former underlying silicon. The LEED pattern observed after annealing at 750 °C indicates the same surface periodicity as recorded for a clean Si surface. Thus the (2×1) reconstruction of the Zr film can be excluded due to the lattice mismatch of Zr and Si.[25,26]

Figure 5(a) shows the curve resolution of the Si 2*p* intensity after annealing at 675 °C. Preset parameters for the curve resolution were the intensity ratio of the Si $2p_{3/2}$/Si $2p_{1/2}$ doublet and its energy separation which were set to $\frac{1}{2}$ and 0.6 eV, respectively.[23,27] Furthermore, the silicon oxide positions of Si^{1+}, Si^{2+}, Si^{3+}, and Si^{4+} with respect to the Si bulk signal were preset according to literature values.[28,29] For the newly formed $ZrSi_2$ component an energy shift of $\Delta E_{kin}=+0.5$ eV with respect to the silicon bulk signal was determined. This energy shift agrees well with $\Delta E_{kin}=+0.6$ eV as reported in literature[30] previously. Thus the curve resolution indicates that $ZrSi_2$ is formed at the sample's surface.

In Fig. 5(b) the curve resolution of the Zr 3*d* intensity after annealing at 675 °C is presented. Within the fitting procedure the intensity ratio of the Zr $3d_{5/2}$ and the Zr $3d_{3/2}$ signals and their energy separation was set to $\frac{3}{4}$ and 2.39 eV, respectively.[22,23] The experimentally determined binding energy of the Zr $3d_{5/2}$ signal is $E_{\mathrm{bin}}=179.2$ eV which is in excellent agreement with the binding energy of $E_{\mathrm{bin}}=179.1$ eV for $ZrSi_2$.[30,31] The $ZrSi_2$ component appearing during annealing is shifted by $\Delta E_{kin}=+3.7$ eV with respect to the position of the ZrO_2. Both the Si 2*p* and the Zr 3*d* separation presented in Figs. 5(a) and 5(b) strongly support a newly formed $ZrSi_2$ compound on the surface which starts to grow for temperatures of 650° and above.

A similar observation of the temperature dependence of ZrO_2 was reported for studies of ZrO_2 films prepared by pulsed laser deposition.[32] However, the transformation temperature from ZrO_2 to $ZrSi_2$ was reported at ~850 °C being slightly higher than the transformation temperature found in our work. Further, a ZrO_2 film grown by pulsed laser deposition leads to the formation of a SiO_2 interlayer. The film thickness of SiO_2 and ZrO_2 were determined being nearly the same.[32,33] It was reported that this system is stable for temperatures up to 880 °C.[32,33] The presence of a SiO_2 interlayer could be a possible explanation for the reported ZrO_2 film stability up to 880 °C. A SiO_2 film on Si is stable for temperatures up to approximately 850 °C. In our investigation the formation of SiO_2 on Si is negligible, since no oxygen was detected at the surface (cf. Fig. 4)

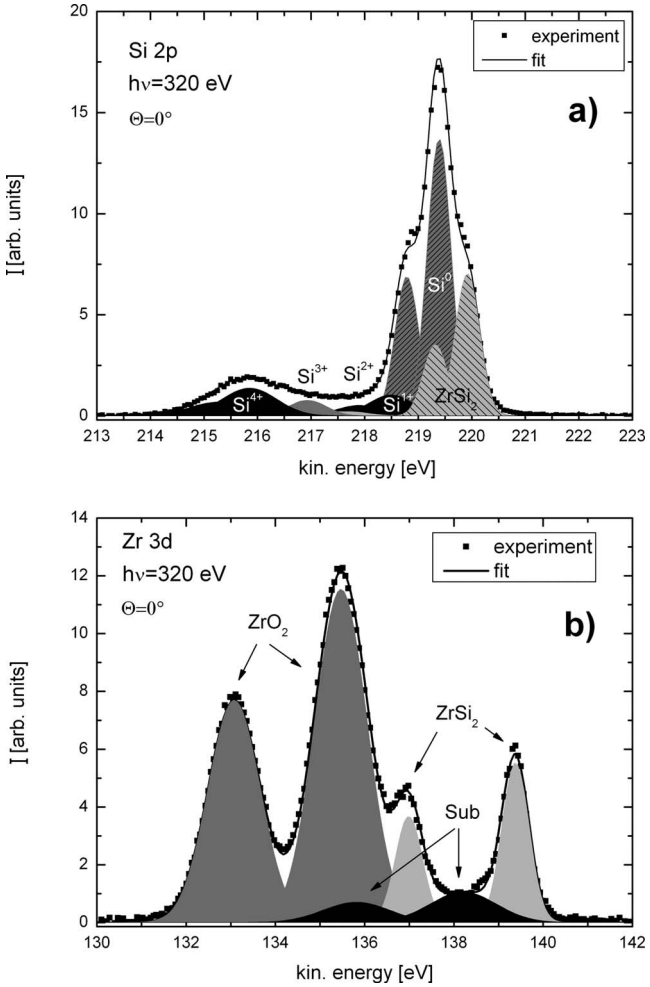

FIG. 5. The curve resolution of the Si 2*p* (a) and Zr 3*d* (b) intensity after annealing at 675 and 650 °C, respectively. (a) The broadening is caused by the formation of $ZrSi_2$, which is shifted by $\Delta E=0.5$ eV to higher kinetic energies within the Si 2*p* spectra. (b) The newly formed $ZrSi_2$ component is shifted by $\Delta E=3.7$ eV to higher kinetic energies within the Zr 3*d* spectra.

The full width at half maximum of the $ZrSi_2$ photoelectron signal is smaller than that of the ZrO_2 signal. This indicates a metallic character of the newly formed component.[32] The broad feature labeled "Sub" in Fig. 5(b) may be composed of several subcomponents lying energetically between ZrO_2 and $ZrSi_2$. A detailed investigation of this component is not possible due to its low intensity compared to the ZrO_2 and $ZrSi_2$ intensities.

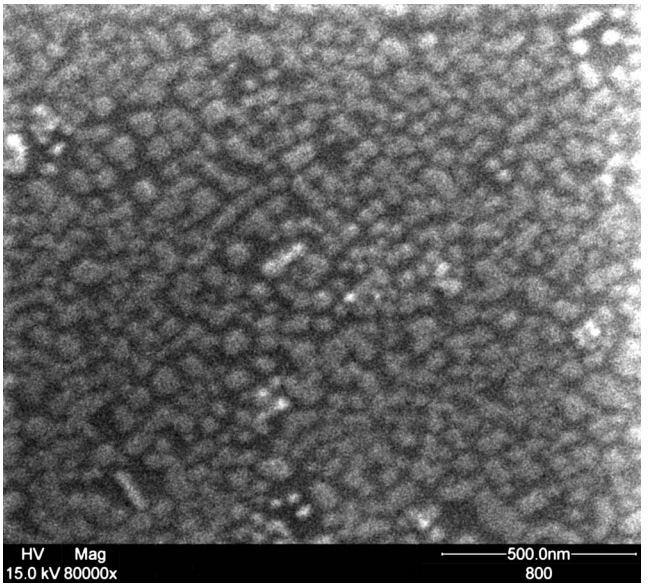

FIG. 6. SEM picture showing the sample surface after annealing at 800 °C. The bright areas indicate $ZrSi_2$ islands formed on the sample surface.

As a complementary surface sensitive method we recorded SEM pictures from the annealed surfaces. The SEM pictures were recorded in order to clarify the question of island formation at the sample surface. Figure 6 displays a SEM picture of the ZrO_2 film showing $ZrSi_2$ islands after annealing at 800 °C. Most of the islands are of round shape with a diameter of ~50–70 nm. Between the island regions bare Si substrate surface areas are displayed. The SEM observation nicely supports the previous discussion based on LEED and XPS data.

In order to investigate the internal structure of the $ZrSi_2$ islands XPD patterns were recorded. Within the simulation the atoms' position were varied and the improvement in the correlation to the experimental pattern was measured by the R-Factor. The model structure modification leading to an improved R-Factor is controlled within a genetic algorithm.

The experimental diffraction patterns presented in Fig. 7 were recorded with a photon energy of $h\nu=320$ eV. Within the analysis it is important to identify new diffraction effects due to the Zr film and to distinguish those from the diffraction signature of the underlying Si substrate. Figures 7(a) and 7(b) show the experimental and simulated diffraction pattern of the Zr $3d$ signal, respectively. The experimental pattern was recorded after ZrO_2 evaporation and sample annealing at 760°.

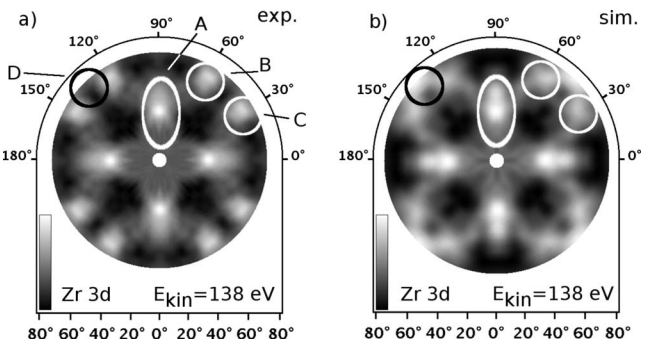

FIG. 7. (a) Experimental and (b) simulated diffraction pattern of a $ZrSi_2$ covered Si surface. (b) The experimental pattern was recorded after evaporation of approximately 11 Å ZrO_2 and annealing at 760 °C. The R-Factor between the two pattern has value of $R=0.11$.

In order to simulate the island formation at the surface a model structure had to be generated. $ZrSi_2$ crystallizes in the base-centered orthorhombic C49 structure, which is also referred to as the zirconium silicide structure.[26] The lattice parameters of the unit cell are $a=3.69$ Å, $b=14.7$ Å, and $c=3.66$ Å. The unit cell of the C49 structure consists of two equivalent stacks which are shifted against each other by a vector of $\frac{\langle a \rangle}{2}$. Each of this stacks consists of three Si layers and two Zr layers. Due to the stacking order every second Si layer in the crystal is actually a doublelayer. The lattice mismatch between the C49 structure along its [011] direction and the Si(100) substrate is ~4.5%. Within the first simulations it became clear that it is not possible to describe the $ZrSi_2$ islands structure on the silicon surface within a C49 structure. A relaxation of the original C49 structure reduced the R-Factor to a value of $R=0.14$. Thus a modification of the Si atoms within the double layer was applied. This variation lead to a modified C49 structure consisting of alternating stacks of Zr doublelayers and three Si layers in between. The surface of this modified structure is terminated by a single layer of Zr atoms. As a consequence of the structure variation the R-Factor was reduced to a value of $R=0.12$.

In order to improve the agreement between experimental and simulated diffraction pattern a further adjustment on the structure model was introduced. The basic idea of this second structure modification of the $ZrSi_2$ film on Si(100) was already applied within a structure search of $HfSi_2$ on Si(100)[34] previously. Thus, as a second step of structure modification a Si doublelayer was introduced terminating the $ZrSi_2$ doublelayer (cf. Fig. 9). Within the simulation the position of the atoms were modified and a lowest R-Factor of $R=0.062$ was found. Figures 7(a) and 7(b) compare the experimental and simulated results, respectively. The excellent

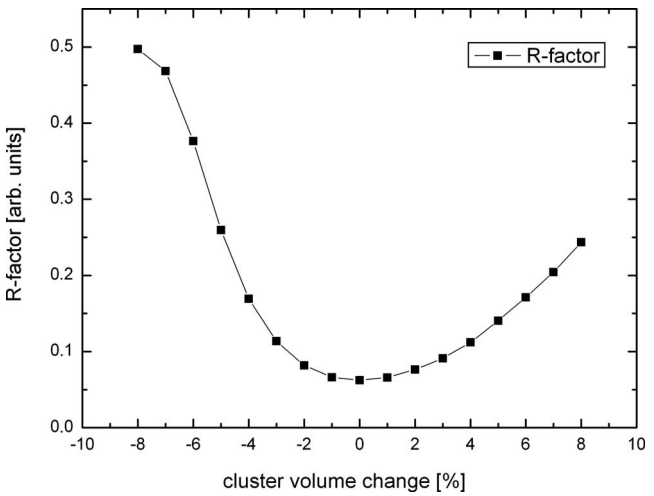

FIG. 8. R-Factor dependence regarding the volume of the cluster. The cluster is scaled in x, y, and z directions by ±8%.

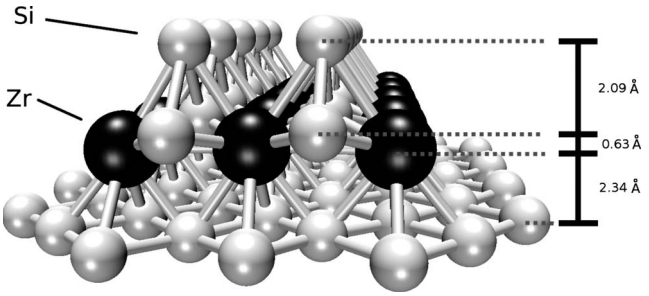

FIG. 9. Structure model used in the simulation for the diffraction pattern of Fig. 7(b). The interlayer distances of Si-Zr, Zr-Si, and Si-Si are ~2.3, ~0.6, and ~2.1 Å, respectively.

agreement between the two patterns is expressed by the position of all diffraction maxima, observed at their respective emission directions. Examples are the elongated maxima "A" close to the center and the bright spots at grazing emission directions "B" and "C." Also, the fine intensity modulation between the prominent intensities is very well reproduced. The origin of the diffraction pattern termed "D" is presently unclear. This feature is displayed in the simulated pattern and is not shown in the experimental data. A possible explanation could be, that this diffraction maximum originates from scattering mainly within the $ZrSi_2$ film parallel to the surface, at grazing emission directions. In the experiment these emission directions are difficult to record, since the spectrometer's accepted area of the sample's surface extends the sample's width. Also, the synchrotron's light spot is distributed over the sample's width due to the grazing incidence.

As a result of the structure search we obtained a model cluster of the $ZrSi_2$ film on Si(100) which consists of 49 atoms and has a diameter of ~16 Å (cf. Fig. 9). The cluster is terminated by a Si doublelayer located ~0.63 Å above the $ZrSi_2$ film and the interdouble layer distance of ~2.1 Å between the Si atoms.

As a test the Si double layer was replaced by a single Si layer terminating the $ZrSi_2$ cluster. In this case the lowest R-Factor obtained was $R=0.14$, being significantly larger than the previous value of $R=0.062$ of the Si double layer termination.

In Fig. 8 the dependence of the R-factor on the cluster size is presented. Clearly, an increased R-Factor is obtained for an increased cluster volume, while the number of atoms contained in the cluster is kept constant. A cluster size variation only 1–2 % already leads to an increased R-Factor of around 10%.

A common way for an estimate of the uncertainty in XPD data is the determination of parameter intervals leading to a 10% increase in the R-Factor.[35] For the 10% estimate we find for the Si doublelayer distance, the Si-Zr distance, and the Zr-Si distance values of 2.09 ± 0.04, 0.63 ± 0.01, and 2.34 ± 0.05 Å, respectively (cf. Table I).

TABLE I. Interlayer distances and calculated errors due to the R-Factor criterion.

Layer	Distance (Å)	Uncertainty (Å)
Si doublelayer	2.09	±0.04
Si-Zr	0.63	±0.01
Zr-Si	2.34	±0.05

IV. CONCLUSIONS

We investigated the temperature stability of thin amorphous ZrO_2 films on Si(100)(2×1) at temperatures ranging from 500 to 750 °C. The total thickness of the investigated films was approximately 11 Å after 75 min of accumulated evaporation time. Annealing of the samples at temperatures higher than 600 °C resulted in the dissociation of ZrO_2 and a simultaneous formation of $ZrSi_2$. After annealing at 725 °C no oxygen remained on the sample and the transformation to $ZrSi_2$ was completed. The formation of $ZrSiO_4$ can be excluded due to the absence of O on the sample. Curve resolutions of the recorded spectra show the formation of $ZrSi_2$ with chemical shifts of $\Delta E_{kin}=+0.5$ and +3.7 eV in the Si 2*p* and the Zr 3*d* signal, respectively. The presumed formation of $ZrSi_2$ islands during annealing was confirmed with SEM pictures. Additionally, the reappearance of the (2×1) reconstruction as observed by LEED indicates that areas of clean Si are terminating the surface. A structure model of the $ZrSi_2$ film is proposed, based on a modified C49 structure. The structure model was obtained from a comprehensive photoelectron diffraction analysis. Within the analysis, a minimum R-Factor of $R=0.062$ reflects excellent agreement between simulated and experimental diffraction data. Further, we propose a Si double layer surface termination of the $ZrSi_2$ islands on the Si(100) surface.

ACKNOWLEDGMENTS

This work was financially supported by the DFG (We 1649/7-1, Germany). Thanks go to the staff of DELTA for continuous support during the beamtimes and to the ISAS Dortmund for providing the SEM pictures.

*frank.schoenbohm@uni-dortmund.de

[1] G. D. Wilk, R. M. Wallace, and J. M. Anthony, J. Appl. Phys. **87**, 484 (2000).
[2] J. P. Locquet, C. Marchiori, M. Sousa, J. Fompeyrine, and J. W. Seo, J. Appl. Phys. **100**, 51610 (2006).
[3] J. Robertson, Eur. Phys. J.: Appl. Phys. **28**, 265 (2004).
[4] M. A. Gribelyuk, A. Callegari, E. P. Gusev, M. Copel, and D. A. Buchanan, J. Appl. Phys. **92**, 1232 (2002).
[5] A. Holleman and E. Wiberg, *Lehrbuch der Anorganischen Chemie* (Walter de Gruyter, Berlin, 1995).

[6] Material-Technologie und Kristalle GmbH, Feinchemikalien und Forschungsbedarf, Chempur, Karlsruhe, 2003.
[7] P. Auger, J. Phys. Radium **6**, 205 (1925).
[8] D. A. Shirley, Phys. Rev. B **5**, 4709 (1972).
[9] C. S. Fadley, Surf. Sci. Rep. **19**, 231 (1993).
[10] D. P. Woodruff and A. M. Bradshaw, Rep. Prog. Phys. **57**, 1029 (1994).
[11] C. Westphal, Surf. Sci. Rep. **50**, 1 (2003).
[12] S. Kono, C. S. Fadley, N. F. T. Hall, and Z. Hussain, Phys. Rev. Lett. **41**, 117 (1978).
[13] S. Dreiner, M. Schürmann, C. Westphal, and H. Zacharias, Phys. Rev. Lett. **86**, 4068 (2001).
[14] S. Dreiner, M. Schürmann, and C. Westphal, Phys. Rev. Lett. **93**, 126101 (2004).
[15] R. Gunnella, F. Solal, D. Sébilleau, and C. R. Natoli, Comput. Phys. Commun. **132**, 251 (2000).
[16] Y. Chen, F. J. García de Abajo, A. Chassé, R. X. Ynzunza, A. P. Kaduwela, M. A. Van Hove, and C. S. Fadley, Phys. Rev. B **58**, 13121 (1998).
[17] ISAS: Institute for Analytical Sciences, Bunsen-Kirchhoff-Str. 11, 44139 Dortmund, Germany.
[18] T. E. Everhart and R. F. M. Thornley, J. Sci. Instrum. **37**, 246 (1960).
[19] A. Sandell, P. G. Karlsson, J. H. Richter, J. Blomquist, P. Uvdal, and T. M. Grehk, Appl. Phys. Lett. **88**, 132905 (2006).
[20] P. G. Karlsson, J. H. Richter, J. Blomquist, P. Uvdal, T. M. Grehk, and A. Sandell, Surf. Sci. **601**, 1008 (2007).
[21] N. Barrett, O. Renault, J.-F. Damlencourt, and F. Martin, J. Appl. Phys. **96**, 6362 (2004).
[22] C. Morant, J. M. Sanz, L. Galán, L. Soriano, and F. Rueda, Surf. Sci. **218**, 331 (1989).
[23] C. Wagner, W. Riggs, L. Davis, J. Moulder, and G. Mullenberg, *Handbook of X-Ray Photoelectron Spectroscopy* (Perkin-Elmer, Eden Prairie, 1978).
[24] L. Kumar, D. D. Sarma, and S. Krummacher, Appl. Surf. Sci. **32**, 309 (1988).
[25] R. Puthenkovilakam, E. A. Carter, and J. P. Chang, Phys. Rev. B **69**, 155329 (2004).
[26] A. Bourret, F. M. d'Heurle, F. K. Le Goues, and A. Charai, J. Appl. Phys. **67**, 241 (1990).
[27] A. Cricenti, G. Le Lay, V. Y. Aristov, B. Nesterenko, N. Safta, J. P. Lacharme, C. A. Sebenne, A. Taleb-Ibrahimi, and G. Indlekofer, J. Electron Spectrosc. Relat. Phenom. **76**, 613 (1995).
[28] S. Dreiner, M. Schürmann, M. Krause, U. Berges, and C. Westphal, J. Electron Spectrosc. Relat. Phenom. **144-147**, 405 (2005).
[29] F. J. Himpsel, F. R. McFeely, A. Taleb-Ibrahimi, J. A. Yarmoff, and G. Hollinger, Phys. Rev. B **38**, 6084 (1988).
[30] T. Yamauchi, H. Kitamura, N. Wakai, S. Zaima, Y. Koide, and Y. Yasuda, J. Vac. Sci. Technol. A **11**, 2619 (1993).
[31] K. Seo, P. C. McIntyre, K. Hyoungsub, and K. C. Saraswat, Appl. Phys. Lett. **86**, 82904 (2005).
[32] J. Okabayashi, S. Toyoda, H. Kumigashira, M. Oshima, K. Usuda, M. Niwa, and G. L. Liu, Appl. Phys. Lett. **85**, 5959 (2004).
[33] J. Okabayashi, S. Toyoda, H. Takahashi, H. Kumigashira, M. Oshima, K. Ikeda, G. L. Liu, Z. Liu, and K. Usuda, e-J. Surf. Sci. Nanotechnol. **4**, 263 (2006).
[34] C. Flüchter, A. de Siervo, D. Weier, M. Schürmann, A. Beimborn, S. Dreiner, M. F. Carazzolle, R. Landers, G. G. Kleiman, and C. Westphal, Surf. Sci. **602**, 3647 (2008).
[35] R. Gunnella, M. Shimomura, F. D'Amico, T. Abukawa, and S. Kono, Phys. Rev. B **73**, 235435 (2006).